

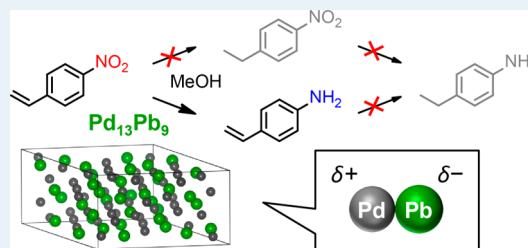
Chemoselective Hydrogenation of Nitrostyrene to Aminostyrene over Pd- and Rh-Based Intermetallic Compounds

Shinya Furukawa,^{*,†} Yurika Yoshida,[†] and Takayuki Komatsu^{*,‡}

[†]Department of Chemistry, [‡]Department of Chemistry and Materials Science, Tokyo Institute of Technology, 2-12-1-E1-10 Ookayama, Meguro-ku, Tokyo 152-8551, Japan

Supporting Information

ABSTRACT: A noble catalytic system based on intermetallic compounds was developed for the chemoselective hydrogenation of *p*-nitrostyrene (NS) to *p*-aminostyrene (AS). The main concept of the catalyst design was to construct polar active sites consisting of two types of metals with different electronegativities. We prepared a series of Pd- and Rh-based intermetallics and investigated their catalytic properties in detail in the catalytic transfer hydrogenation of nitrobenzene and NS in the presence of 4-methyl-1-cyclohexene (MC) or methanol as a hydrogen donor. FT-IR studies of adsorbed CO confirmed that the number of Pd ensembles exposed on a surface was greatly decreased by the formation of an intermetallic phase; hence, the particle surface consisted of two metal elements being coadjacent at the atomic level. The product distribution achieved with Pd catalysts was dependent on the electronegativity of the second metal element: more electronegative metals gave higher AS selectivity and lower *p*-ethylnitrobenzene selectivity. Rh catalysts selectively gave AS, and their AS yields increased as the electronegativity of the second metal increased. The results revealed that an increase in the electronegativity of the second metal element provided polar sites and enhanced the activation of methanol as a hydrogen donor, which accelerated the hydrogenation of the nitro group of NS and, hence, improved the yield of AS. The high selectivity of Rh catalysts was due to the absence of MC activation ability, which caused the hydrogenation of the vinyl group of NS. Pd₁₃Pb₉ exhibited the highest chemoselectivity toward AS (92%) among the investigated Pd catalysts. Moreover, RhPb₂ exhibited not only high AS selectivity (93%) but also the highest NS conversion (94%) among the investigated catalysts. RhPb₂ also exhibited high selectivity toward AS (91%), even when H₂ was used as a hydrogen source. Thus, intermetallics that contain Pb, which was the most electronegative metal used in this study, afforded good catalytic performance and were observed to be good catalysts for the chemoselective hydrogenation of NS.



KEYWORDS: intermetallic, chemoselective, nitrostyrene, catalytic transfer hydrogenation, polarity

1. INTRODUCTION

Selective hydrogenation of nitro groups in the presence of other reducible functional groups is an important chemical transformation to obtain functionalized anilines as important intermediates for pharmaceuticals, polymers, herbicides, and other fine chemicals.^{1,2} Selective hydrogenation has typically been performed using a stoichiometric amount of reducing agents,^{2–5} which produces a large amount of waste byproducts. In view of the principles of green chemistry, the development of a heterogeneous catalytic system for the chemoselective hydrogenation of nitro compounds is desirable; however, conventional platinum-group metal catalysts hydrogenate not only the nitro group but also any olefinic or carbonyl functional groups.⁶ Currently, only a few catalytic systems that involve nanoparticulate Au^{7,8} or Ag^{9,10} supported on specific oxides have achieved the chemoselective hydrogenation of nitro aromatic compounds, such as nitrostyrene into aminostyrene. The high selectivities of these catalysts have been explained by the formation of charged hydrogen species (H⁺ or H⁻) at the metal–support interface; these species are active toward the reduction of the polar nitro group, but are inactive toward the reduction of the nonpolar C=C bond.^{8–11} In the case of these

supported metal catalysts, however, such interfacial sites are limited to only a small portion of the exposed surface metal atoms. Mitsudome et al. designed a core–shell-structured Ag–CeO₂ nanocomposite with high chemoselectivity because of its maximized fraction of interfacial sites.⁹

In this context, an ideal structure for chemoselective hydrogenation would be an arrangement of interfacial sites that exhibit high order at the atomic level. One of the promising candidates for such a material is an intermetallic compound. Intermetallic compounds are stoichiometric compounds of two or more metal elements; they have specific crystal structures, highly ordered surface atomic arrangements, and modified electronic structures compared with the parent metals.¹² Therefore, an appropriate combination of two metal elements with different electronegativities would provide an ideal arrangement of active sites to generate partially charged hydrogen species and to exhibit high chemoselectivity. In the case of hydrogenation of α,β -unsaturated aldehyde to the

Received: January 20, 2014

Revised: March 20, 2014

Published: March 24, 2014

corresponding alcohol, it was reported that an increase in polarity of the catalyst surface indeed enhanced the chemoselectivity.¹³ In addition to structural design, the choice of reducing agent is also an important factor governing chemoselective hydrogenation. The use of gaseous hydrogen (H_2) as a reducing agent typically requires a high pressure of hydrogen and a special apparatus.^{7–10} Moreover, the reduction of both nitro and olefinic groups often occurs over platinum-group metal catalysts.⁶ In contrast, catalytic transfer hydrogenation (CTH) using an appropriate hydrogen donor instead of H_2 makes handling easier and improves the selectivity of the reaction.^{14–17} Among the platinum-group metals, Pd and Rh have been reported to exhibit high catalytic activities in CTH reactions of organic compounds.^{17,18}

In this study, we prepared a series of Pd- and Rh-based intermetallic compounds supported on silica and investigated their catalytic properties in CTH of *p*-nitrostyrene (NS). To better understand the hydrogenation of the nitro group, we also performed CTH of nitrobenzene in addition to that of NS. Herein, we report our development of chemoselective intermetallic catalysts and the dependence of the activity and selectivity of these catalysts on their electronic and geometric characteristics.

2. EXPERIMENTAL SECTION

2.1. Catalyst Preparation. Pd/SiO₂ was prepared by a pore-filling impregnation. An aqueous solution of Pd(NO₃)₂ (4.8×10^{-2} g·mL⁻¹, 0.64 mL, N.E. ChemCat) was diluted with ion-exchanged water and added to silica gel (5.0 g, Cariact G-6, Fuji Silysia Co.) that had been previously dried at 403 K and cooled in air to room temperature. The amount of palladium solution was calculated to fill the pores of the silica gel and to achieve the palladium loading of 3 wt %. The mixture was sealed by a piece of plastic film overnight at room temperature. It was then dried over a boiling water bath with stirring, followed by calcination under dry at 403 K for 1 h and then at 673 K for 1 h. After the calcination, the catalyst was reduced under flowing H_2 (60 mL·min⁻¹, 99.9995%, Taiyo Nippon Sanso) at 403 K for 1 h and then at 673 K for 2 h. The catalyst was cooled to room temperature with flowing helium and kept in a drying desiccator.

In a similar manner, Rh/SiO₂ (Rh 3 wt %) was also prepared by using an aqueous solution of Rh(NO)(NO₃)₃. Intermetallic catalysts, Pd–M/SiO₂ (M = Cu, Ga, Pb, and Zn) and Rh–M'/SiO₂ (M' = Fe, Ni, Pb, Sb, Sn, and Ti), were prepared by a successive impregnation with Pd/SiO₂ and Rh/SiO₂, respectively. In the case of Pd–Cu (1:1), an aqueous solution of Cu(NO₃)₂·3H₂O (99%, Kanto) was added to Pd/SiO₂ so that the atomic ratio of Pd/Cu was adjusted to 1. The mixture was sealed by a piece of plastic film overnight at room temperature. It was then dried over a boiling water bath with stirring, followed by reduction under flowing H_2 (99.9995%, Taiyo Nippon Sanso) at 1073 K for 1 h.

Other intermetallic catalysts were prepared in a similar way at 773, 873, or 1073 K of reduction temperature using a specific amount of the second metal precursor: Ga(NO₃)₃·8H₂O, Pb(NO₃)₂Zn(NO₃)₂·6H₂O, Fe(NO₃)₃·9H₂O, Ni(NO₃)₂·6H₂O, SbCl₃, SnCl₂·2H₂O, and TiCl₄(THF)₂. In the case of TiCl₄(THF)₂, THF was used as the solvent instead of water. Other intermetallic catalysts, Pd–M/SiO₂ (M = Bi, Fe, and Sn) and RhBi/SiO₂, were prepared by coimpregnation with mixed aqueous solution of Pd(NO₃)₂ or Rh(NO)(NO₃)₃ and the second metal precursor: Bi(NO₃)₃·5H₂O, Fe(NO₃)₃·9H₂O,

and SnCl₂·2H₂O. The composition ratio and the reduction temperature of each intermetallic catalyst are as follows: Pd–Bi (3:1), 1073 K; Pd–Cu (1:1), 1073 K; Pd–Fe (1:1), 773 K; Pd–Ga (13:5), 873 K; Pd–Ga (5:3), 1073 K; Pd–Ga (1:1), 1073 K; Pd–Pb (1:1), 1073 K; Pd–Sn (3:1), 773 K; Pd–Zn (1:1), 1073 K; Rh–Bi (1:1), 773 K; Rh–Fe (1:1), 1073 K; Rh–Ni (1:1), 1073 K; Rh–Pb (3:2), 1073 K; Rh–Pb (1:1), 873 K; Rh–Pb (1:2), 1073 K; Rh–Sn (2:1), 1073 K; Rh–Ti (3:1), 1073 K. We carried out the reduction treatment at high temperature with SiO₂ support itself to investigate the effect of sintering of the support. N₂ adsorption experiments before and after the treatment (at 1073 and 873 K) revealed that only a slight sintering occurred at 1073 K (S_{BET} : 673 → 622 m²·g⁻¹), whereas no sintering was observed at 873 K (S_{BET} : 673 → 686 m²·g⁻¹). Therefore, the treatment does not seem to result in a considerable effect to the catalytic performances.

2.2. CTH Reaction. CTH reaction was carried out in a 100 mL, three-necked, round-bottom flask equipped with a reflux condenser and a gas balloon. Prior to the reaction, catalyst (250 mg) was reduced in the reactor under flowing H_2 (60 mL·min⁻¹) at 723 K for 0.5 h using a mantle heater. After the reduction pretreatment, the reactor was cooled to room temperature, and the atmosphere was completely replaced by dry Ar. A methanol solution (5.0 mL) of nitrobenzene (0.50 mmol) or NS (0.25 mmol) was added into the reactor through a silicone septum. The reaction was initiated by adding 4-methyl-1-cyclohexene (0.75 mmol) as a hydrogen donor at 343 K. In the case of monometallic Pd/SiO₂ and Rh/SiO₂, the catalyst amount and reduction temperature were 150 mg and 573 K, respectively. The products in the liquid phase were identified by gas chromatograph mass spectroscopy (GC–MS, JEOL, Automass System II) and quantitated by flame ionization detection gas chromatograph (FID–GC, Shimadzu, GC-14B) equipped with a capillary column (GL Sciences, TC-17, 0.25 mm × 30 m) using *n*-dodecane as an internal standard: nitrostyrene, m/z = 149.0 (149.1 calcd); aminostyrene, m/z = 119.0 (119.1 calcd); ethylnitrobenzene, m/z = 151.0 (151.1 calcd); ethylaniline, 121.0 (121.1 calcd); *N*-methylaminostyrene, m/z = 133.0 (133.1 calcd); *N*-methylenestyrylamine, m/z = 131.0 (131.1 calcd.). Gaseous products were analyzed by a thermal conductivity detection gas chromatograph (TCD–GC, Shimadzu, GC-14B) equipped with a packed column (GL Sciences, Active Carbon). We confirmed that material balance was almost equal to 1 (0.97–1.03) in the typical reaction condition. Conversion of the reactant and selectivity to a certain product were defined as follows: conversion (%) = [(initial concentration of the reactant) – (concentration of the reactant after reaction)]/(initial concentration of the reactant) × 100, selectivity (%) = (concentration of the product)/(total concentration of the all products) × 100.

2.3. Characterization. The crystal structure of supported metal and intermetallic particles was examined by powder X-ray diffraction (XRD) with a Rigaku RINT2400 using an X-ray source of Cu K α . Difference XRD patterns were obtained by subtraction of the pattern of silica support from those of the prepared catalysts so that the baseline was flattened. Transmission electron microscopy (TEM) was conducted on a JEOL JEM-2010F at the accelerating voltage of 200 kV. To prepare the TEM specimen, all samples were sonicated in tetrachloromethane and then dispersed on a copper or molybdenum grid supported by an ultrathin carbon film. Selected area electron diffraction (SAED) patterns were acquired with a 20- μ m-sized area aperture and a camera distance of 30 cm. The camera

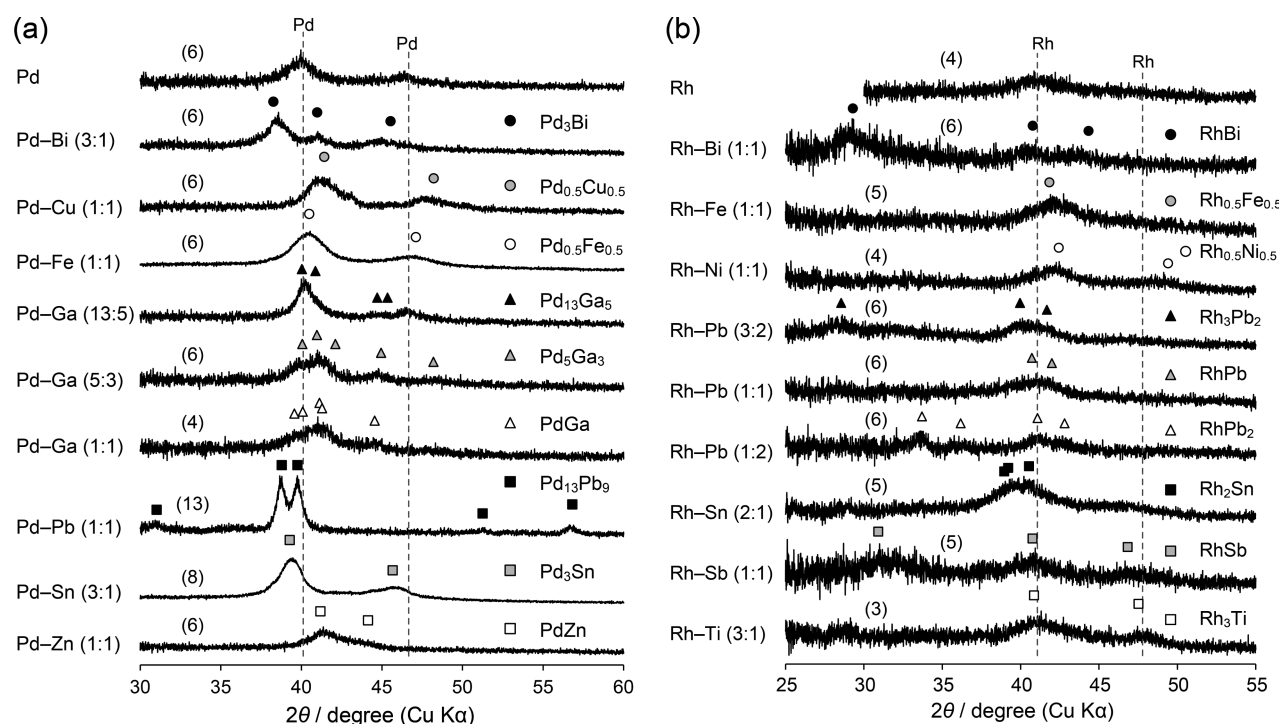


Figure 1. XRD patterns of the prepared (a) Pd- and (b) Rh-based intermetallic compounds supported on silica. Figure in parentheses indicates the crystallite size estimated by Scherrer's equation.

constant was calibrated by using an authentic Pt/ Al_2O_3 (Pt: 3 wt %) for determination of reflection indices. Fourier transformed infrared (FT-IR) spectra of adsorbed CO were measured with a JASCO FT/IR-430 spectrometer in transmission mode. A self-supporting wafer ($\sim 20 \text{ mg}\cdot\text{cm}^{-2}$) of catalyst was placed in a quartz cell with CaF_2 windows and attached to a glass circulation system. The catalyst was reduced at 723 K for 0.5 h with 20 kPa of circulating hydrogen through a cold trap kept at 77 K. Then the catalyst was evacuated at the same temperature for 0.5 h, followed by cooling to room temperature. In the case of monometallic Pd/ SiO_2 , the temperature of the reduction and evacuation was kept at 573 K. CO (2.0 kPa) was introduced for 30 min and then evacuated. Spectra were recorded with 1 cm^{-1} of resolution before and during the evacuation at intervals of 5 min. X-ray photoelectron spectra (XPS) of the intermetallics were recorded with an ULVAC PHI 5000 VersaProbe spectrometer. The catalyst was pressed into a pellet and placed into a quartz reactor, where it was reduced under flowing hydrogen (50 mL min^{-1}) at 673 K for 0.5 h prior to the measurement. Spectra were obtained with an Al $K\alpha$ X-ray source using C 1s as a reference for binding energy.

3. RESULTS AND DISCUSSION

3.1. Characterizations of Catalysts. Figure 1 shows the XRD patterns of the prepared (a) Pd- and (b) Rh-based catalysts. In the case of Pd–Bi (3:1), diffraction peaks assigned to the intermetallic phase Pd_3Bi ($2\theta = 38.3^\circ$, 39.6° , and 41.0°) were observed, and no residual monometallic Pd phase was detected. Similarly, in most cases, the desired intermetallic or alloy phases were formed as single phases with composition ratios identical to the loaded ratios. The catalyst of Pd–Pb (1:1) exclusively gave $\text{Pd}_{13}\text{Pb}_9$ phase, indicating that a portion of Pb atoms did not participate in the intermetallic formation and remained as small clusters that were not detectable by

XRD. Only the preparation of Pd–Ga (13:5) resulted in the formation of a mixture of $\text{Pd}_{13}\text{Ga}_5$ and monometallic Pd. The crystallite sizes of the intermetallic particles in the catalysts were estimated by the Scherrer equation using the most intense diffraction peaks. The sizes were typically within 4–6 nm, with the exception of $\text{Pd}_{13}\text{Pb}_9$ (13 nm). Notably, most of the prepared intermetallic catalysts exhibited similar particle sizes. This similarity is partly because most of the intermetallics were prepared by successive impregnation, in which the resulting particle size should depend on the size of the parent monometallic particle. Figure 2 shows the TEM image and

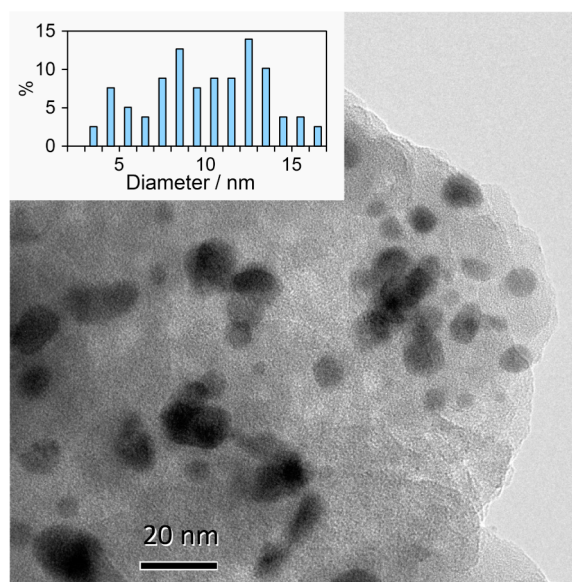


Figure 2. TEM image of $\text{Pd}_{13}\text{Pb}_9/\text{SiO}_2$. Inset shows size distribution of intermetallic nanoparticles.

size distribution of Pd₁₃Pb₉. The particles were mainly 8–13 nm in size, and the particles of 13 nm exhibited the highest population. This result agrees with the estimation based on the Scherrer equation. No small particles with a diameter <3 nm were observed. Similar results were observed for Rh-based intermetallic, RhPb₂, as shown in Figure 3. The sizes of RhPb₂

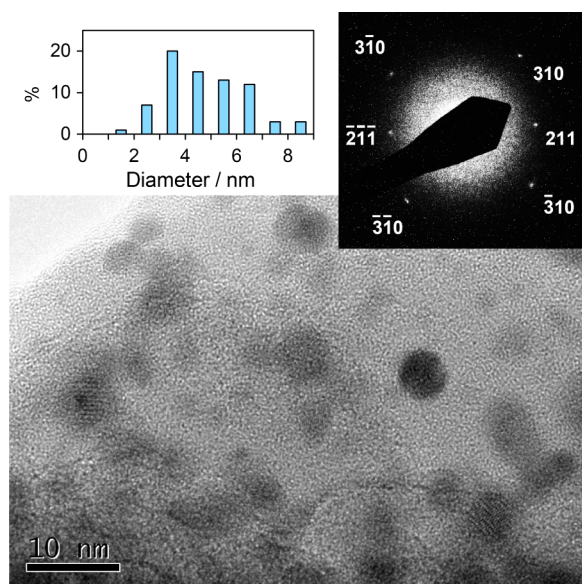


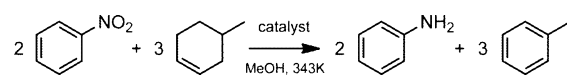
Figure 3. TEM image of RhPb₂/SiO₂. Left and right insets show size distribution of intermetallic nanoparticles and SAED pattern of a single particle, respectively.

particles were predominantly within 3–6 nm, which is roughly consistent with the estimated values. The sample contained very few particles that were hardly detectable by XRD (<2 nm). In the case of RhPb₂, its XRD pattern appeared somewhat broad; we therefore further characterized this sample. Selected-area electron diffraction was performed on a single RhPb₂ particle with a size of ~6 nm (Figure 3, upper-right inset). Diffraction spots characteristic to RhPb₂ (space group *I4/mcm*) were observed, which clearly indicates that the particle was a single crystal of intermetallic RhPb₂. The observed 211 and 310 diffractions correspond to the peaks at 33.7° and 42.8° in the XRD pattern, respectively.

3.2. CTH Reaction of Nitrobenzene. The prepared catalysts were then applied to CTH reactions. First, several hydrogen donors were examined in the CTH reaction of nitrobenzene to aniline over Pd/SiO₂ to identify an appropriate hydrogen donor. The reaction did not proceed when methanol or 2-propanol was used as a hydrogen donor. In contrast, a moderate conversion (49%) without the evolution of H₂ was achieved when 4-methyl-1-cyclohexene (MC) was used. Although formic acid (95%) and ammonium formate (70%) gave higher conversions than MC, H₂ was detected in the gas phase. The formation of H₂ suggests that hydrogenation by H₂ also occurred in addition to the CTH reaction. Therefore, we selected MC as an appropriate hydrogen donor in the present study.

CTH reactions between nitrobenzene and MC using various catalysts were performed to evaluate their catalytic abilities toward the hydrogenation of a nitro group (Table 1). In the case of Pd catalysts (except Pd₃Bi), nitrobenzene and MC were selectively converted into aniline and toluene, respectively.

Table 1. CTH Reaction of Nitrobenzene over Pd- and Rh-Based Intermetallic Compounds Supported on SiO₂^a



entry	catalyst	D/Nm ^b	conversion (%)		selectivity (%)	
			nitrobenzene	MC	aniline	toluene
Pd–M/SiO ₂						
1	Pd	6	49	54	>99	>99
2 ^c			0			
3	Pd ₁₃ Ga ₅		14	27	90	99
4 ^d	Pd ₅ Ga ₃	6	13	35	>99	>99
5 ^c			<1			
7	PdFe	6	8	10	>99	>99
8	PdZn	6	7	16	>99	>99
9	PdGa	4	6	11	87	98
10	PdCu	6	5	17	>99	>99
11	Pd ₃ Sn	8	5	6	65	>99
12	Pd ₃ Bi	6	0	0		
Rh–M'/SiO ₂						
13	Rh	4	0	<1		
14	Rh ₃ Pb ₂	6	63	5	87	>99
15 ^c			58		87	
16	RhPb	6	92	0	92	
17	RhPb ₂	6	94	0	>99	
18	RhSb	5	15	5	89	>99
19	RhBi	6	13	0	>99	
20 ^c			13		>99	
21 ^{c,e}			0			
22	Rh ₂ Sn	5	10	0	>99	
23	Rh ₃ Ti	3	0	0		

^aReaction conditions: catalyst, 150 mg (monometallic Pd and Rh) or 250 mg (Pd–M and Rh–M' intermetallics); solvent, 5 mL (methanol); temp, 343 K; time, 1 h. ^bD: crystallite size estimated by Scherrer's equation. ^cWithout MC. ^dThe catalyst contains monometallic Pd phase. ^eTHF was used as a solvent instead of methanol.

Moreover, the CTH reaction did not proceed in the absence of MC (entries 2 and 5). These results indicate that the CTH reaction from MC to nitrobenzene occurred; however, the conversions of MC were higher than those of nitrobenzene in all cases (entries 1–11). The observed higher conversions of MC imply an involvement of the simple dehydrogenation of MC to form toluene and H₂. In some cases (entries 3, 9, and 11), small amounts of *N*-methylaniline and methylcyclohexane were formed as byproducts from nitrobenzene and MC, respectively. The formation of *N*-methylaniline was not observed when tetrahydrofuran (THF) was used as a solvent (data not shown), suggesting that methanol was involved in the methylation of aniline. The presence of methylcyclohexane indicates that the self-CTH reaction of MC into toluene and methylcyclohexane occurred.

Rh catalysts exhibited catalytic properties that differed from those of Pd catalysts. Rh/SiO₂ was not active toward the CTH reaction (entry 13). This result is surprising because Rh has been reported to be an effective catalyst for CTH reactions.¹⁷ A possible reason for the low activity of Rh/SiO₂ is the presence of nitro groups, which can strongly bind to monometallic Rh sites. To investigate the effect of nitro groups, we performed the self-CTH reaction of MC in the presence and absence of nitrobenzene (Supporting Information, Table S1). In the case of Pd/SiO₂, although MC conversion decreased by half, the reaction proceeded even in the presence of nitrobenzene. Rh/

SiO₂ gave a MC conversion similar to that of Pd/SiO₂ in the absence of nitrobenzene, consistent with the previously reported results.¹⁷ However, in contrast, the reaction did not occur at all in the presence of nitrobenzene. These results indicate that the nitro group fatally poisons the monometallic Rh sites and thereby inhibits the activation of methanol. Although the hydrogenation of nitrobenzene to aniline proceeded over Rh-based intermetallic catalysts, the dehydrogenation of MC to toluene scarcely occurred (entries 14, 16–19, 22, and 23). Moreover, the hydrogenation of nitrobenzene occurred even in the absence of MC (entries 15 and 20), with the nitrobenzene conversion almost maintained. However, no reaction occurred when THF was used as a solvent instead of methanol (entry 21). These results suggest that methanol functions as a hydrogen donor over Rh-based intermetallic catalysts, whereas MC does not.

The conversion of nitrobenzene on Pd- and Rh-based intermetallic catalysts differed, although the crystallite sizes of these catalysts were similar. We subsequently investigated the difference in their catalytic activities in terms of geometric and electronic effects. Figure 4 shows the dependences of their

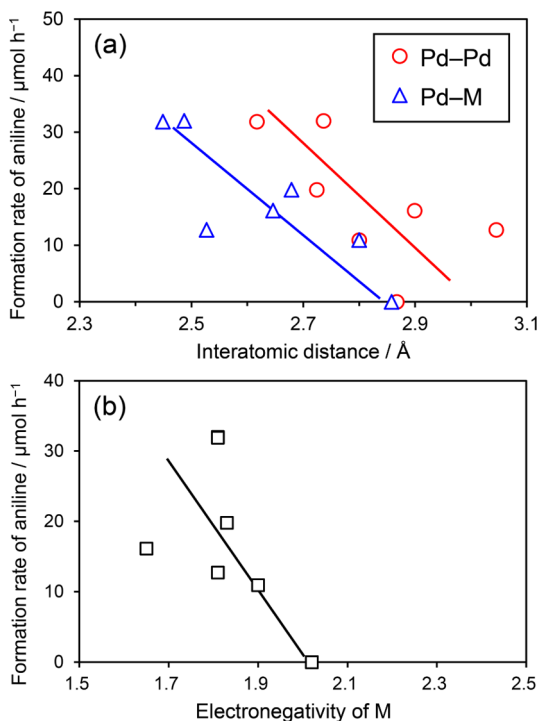


Figure 4. Dependences of the formation rate of aniline on (a) the interatomic distance of the nearest Pd–Pd or Pd–M and on (b) the electronegativity of M.

catalytic activities on (a) the interatomic distance between the nearest Pd–Pd or Pd–M and on (b) the electronegativity of the second metal. In the present study, we employed Allred–Rochow electronegativity,^{19,20} which has been regarded as a valid scale to discuss electron distribution in a compound.²¹ Allred–Rochow electronegativity depends on the surface electric field on an atom (eZ_{eff}/r^2 , where e is the elementary charge, Z_{eff} is the effective nuclear charge, and r is the covalent radius)^{20,21} and, hence, considers the difference in covalent radii. Especially in the case of intermetallic compounds, it is very important to take the difference in covalent radii into account because the difference is not so small (for example: Pd,

1.31 Å; Rh, 1.35 Å; Ga, 1.26 Å; Pb, 1.47 Å). The formation rate of the product, here aniline, was used as the scale of the catalytic activity. Shorter interatomic distances were correlated with higher reaction rates, which indicates that the geometric factor of the catalysts affects their catalytic activity. This correlation is consistent with the common hypothesis that longer Pd–Pd distances should increase the energy barrier of C–H bond dissociation. A weak negative correlation was also observed between the catalytic activity and the electronegativity of the second metal, that is, electron-rich Pd affords greater catalytic activity. A possible interpretation of this result is that electron-rich Pd atoms enhance back-donation to antibonding orbitals of C–H bond, which facilitates the dissociation of the bond.

A similar study was also performed on Rh-based intermetallic catalysts, as shown in Figure 5. In contrast to Pd series, no

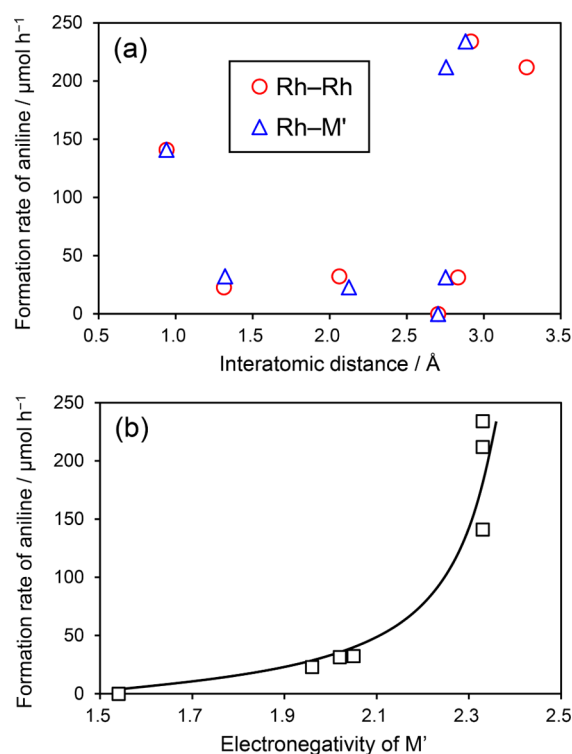


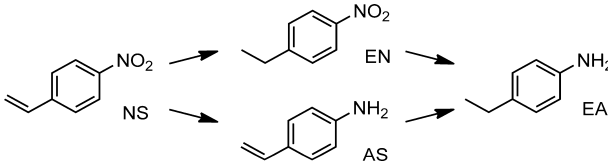
Figure 5. Relationship between the formation rate of aniline and (a) the interatomic distance of the nearest Rh–Rh or Rh–M' and (b) the electronegativity of M'.

apparent relationship was observed between the catalytic activity and interatomic distance (Figure 5a); however, a positive correlation was observed with respect to the electronegativity of the second metal (Figure 5b). As previously discussed, Rh catalysts require O–H activation of methanol to trigger the reaction. According to the literature,^{22,23} O–H dissociation of methanol in a homolytic fashion on nonpolar metallic sites is highly endothermic and therefore kinetically unfavorable; however, this dissociation is essentially thermo-neutral²⁴ or exothermic^{25,26} on polar sites, such as oxide ions in a heterolytic fashion. Actually, in the case of a reported CTH system of styrene and 2-propanol over Cu/Al₂O₃,²⁷ the authors proposed that O–H activation of 2-propanol occurs on the basic site of Al₂O₃ but not on metallic Cu. In our catalytic system, a positive kinetic isotope effect ($k_{\text{H}}/k_{\text{D}} = 7.2$) was observed when deuterated methanol (CH₃OD) was used

instead of nondeuterated methanol (CH_3OH) in CTH reaction over Rh_3Pb_2 , which indicates that the rate-determining step is O–H dissociation of methanol. Therefore, the increase in the catalytic activity with increasing electronegativity is attributed to the enhancement of the activation rate of methanol, which is probably due to the formation of polar sites via the incorporation of electronegative atoms. Thus, the significant factor to determine the catalytic activity was different between the Pd and the Rh catalysts.

3.3. CTH Reaction of NS. We subsequently performed CTH reactions of NS using the prepared catalysts (Table 2).

Table 2. CTH Reaction of *p*-Nitrostyrene (NS) over Pd- and Rh-Based Intermetallic Compounds Supported on SiO_2 ^a



entry	catalyst	D/Nm ^b	conv. of NS (%)	selectivity (%)		
				AS	EN	EA
Pd–M/SiO ₂						
1	Pd	6	100	0	63	26
2	Pd ₁₃ Ga ₅ ^b		22	0	>99	0
3 ^c	Pd ₅ Ga ₃	6	14	0	82	18
4 ^{c,d}			<1	0	>99	0
5	Pd ₁₃ Pb ₉	13	10	93	5	2
6 ^d			10	93	4	3
7	Pd ₃ Bi	6	10	43	27	25
8	PdZn	6	7	0	>99	0
9	PdGa	4	5	0	>99	0
10	PdFe	6	2	55	45	0
11	Pd ₃ Sn	8	<1			
Rh–M'/SiO ₂ ^d						
12	Rh	4	<1	0	>99	0
13	RhPb ₂	6	94	93	6	1
14 ^e			95	95	0	1
15 ^f			0			
16 ^g			36	91	5	4
17	RhPb	6	38	94	0	0
18	Rh ₃ Pb ₂	6	15	>99	0	0
19	RhBi	6	14	>99	0	0
20	Rh ₂ Sn	5	6	>99	0	0
21	RhSb	5	3	95	5	0
22	RhFe	5	0			
23	Rh ₃ Ti	3	0			

^aReaction conditions: catalyst, 150 mg (monometallic Pd and Rh) or 250 mg (Pd–M and Rh–M' intermetallics); solvent, 5 mL (methanol); temperature, 343 K; time, 1 h. ^bD: crystallite size estimated by Scherrer's equation. ^cThe catalyst contains monometallic Pd phase. ^dWithout MC. ^eWith MC. ^fStyrene was used as a substrate. ^gH₂ (60 mL min⁻¹) and THF were used as a hydrogen donor and a solvent, respectively, with 0.5 h of reaction time.

MC was used as a hydrogen donor only with Pd catalysts. In this reaction, NS undergoes the hydrogenation of its nitro or vinyl group to form *p*-aminostyrene (AS) or *p*-ethylnitrobenzene (EN), respectively. Overhydrogenation of these products also occurs to yield *p*-ethylaniline (EA). Pd/SiO₂ gave EN with moderate selectivity, and overhydrogenation to EA also occurred (entry 1). These results are consistent with those

reported for monometallic Pd and Pt catalysts. The conversions of Pd-based intermetallic catalysts were lower than those of Pd/SiO₂ catalyst. Pd-based intermetallic catalysts were divided into two categories in terms of their product distribution: Pd₁₃Ga₅, Pd₅Ga₃, PdGa, and PdZn selectively gave EN (entries 2, 3, 8, and 9), whereas Pd₁₃Pb₉, Pd₃Bi, and PdFe dominantly gave AS (entries 5, 7, and 10). Notably, Pd₁₃Pb₉ exhibited high chemoselectivity to AS (93%, entry 5). In the absence of MC, the CTH reaction of NS did not occur over the EN-selective catalyst Pd₅Ga₃ (entry 4), similar to the previously discussed case of nitrobenzene hydrogenation. Surprisingly, however, the AS-selective catalyst Pd₁₃Pb₉ exhibited a similar catalytic performance in the absence of MC (entry 6). The high selectivity exhibited by Pd₁₃Pb₉ was maintained even when the conversion reached 99% (Supporting Information, Figure S1).

Rh/SiO₂ exhibited very low catalytic activity and yielded EN selectively (entry 12). Rh-based intermetallic catalysts, in contrast, gave AS with high selectivities (entries 13, 17–21). The intermetallic catalysts with Fe and Ti did not catalyze the CTH reaction (entries 22 and 23). The catalytic activity of Rh catalysts depended on the second metal element, as was the case with nitrobenzene hydrogenation. Notably, RhPb₂ exhibited high NS conversion (94%) and chemoselectivity toward AS (93%) and was the most effective intermetallic catalyst for the chemoselective hydrogenation of NS to AS (entry 13). The addition of MC to the reaction with RhPb₂ did not affect its catalytic performance (entry 14). Moreover, the self-CTH reaction of NS in the absence of NS did not occur (data not shown). These results indicate that MC is a spectator and is not activated by RhPb₂. Furthermore, the CTH reaction of styrene with methanol did not proceed over RhPb₂ (entry 15), which revealed that the vinyl group was not hydrogenated by hydrogen species derived from methanol. On the basis of the results, we conclude that the difference in the actual hydrogen donor determines which functional group of NS is hydrogenated: the CTH reaction with MC gave EN, and that with methanol gave AS. The catalytic performance of RhPb₂ was also examined in the simple hydrogenation of NS with H₂. High selectivity toward AS (91%) was obtained even with H₂ (entry 16), which revealed the potential applicability of the intermetallic compound for chemoselective hydrogenation using H₂.

To investigate the further applicability of the catalysts, we performed the chemoselective hydrogenation of various nitro aromatic compounds containing olefinic bonds using the most selective Pd₁₃Pb₉ and RhPb₂ catalysts, as shown in Table 3. The reaction involving Pd₁₃Pb₉ catalyst was performed at 363 K to increase the reaction rate. As shown in Supporting Information Figure S1, NS was converted into AS almost quantitatively in 6 h (entry 1, 96% yield). RhPb₂ exhibited much higher catalytic activity (100% conversion within 1 h), whereas the selectivity was slightly lower than that of Pd₁₃Pb₉ (entry 2). Similar results were obtained when 3-nitrostyrene was used as a substrate (entries 3 and 5). These results are consistent with the result that styrene was not hydrogenated under these experimental conditions, as previously discussed. Since the hydrogen species formed on these catalysts do not hydrogenate the vinyl group, its hydrogenation should be suppressed, irrespective of the vinyl group's position. After the reaction, these catalysts were separated from the reaction mixture via simple decantation and were reused without any loss of catalytic activity or selectivity (entries 4 and 6). Other nitroaromatic compounds, such as 4-nitrostilbene and nitroindole isomers, were also tested using

Table 3. Chemoselective Hydrogenation of Various Nitroaromatic Compounds Having Olefinic Bonds into Amino Derivatives Using Pd₁₃Pb₉/SiO₂ and RhPb₂/SiO₂^a

entry	substrate	Product	catalyst	temp / °C	time / h	conv. (%)	sel. (%)
1			Pd ₁₃ Pb ₉	90	6	99	96
2			RhPb ₂	70	1.5	100	92
3			Pd ₁₃ Pb ₉	90	5	99	96
4			reuse	90	5	99	96
5			RhPb ₂	70	1	100	90
6			reuse	70	1	100	90
7 ^b			RhPb ₂	70	1	100	99
8			RhPb ₂	70	1	100	96
9			RhPb ₂	70	1	100	96
10			RhPb ₂	70	1	100	96

^aReaction conditions: catalyst, 250 mg; solvent, 5 mL (methanol); atmosphere, 1 atm Ar. MC was not used in these reactions. ^bSolvent, 15 mL (methanol).

RhPb₂ as a catalyst and were selectively converted into the corresponding amino derivatives within 1 h (entries 7–10). As was the case of nitrostyrenes, no difference in selectivity was observed in the case of 6-, 5-, and 4-nitroindoles. Thus, these catalysts have broad applicability for the chemoselective hydrogenation of nitroaromatic compounds.

We subsequently studied the geometric and electronic effects on the catalytic performance to understand the factors that govern the catalytic activity and product distribution. Figure 6 shows the dependence of the formation rate of the product on the interatomic distance of (a) Pd–Pd in Pd catalysts and (b) Rh–Rh in Rh catalysts. Negative correlations with interatomic distance were observed among the EN-selective catalysts (Figure 6a, circle). This trend is consistent with the results of the hydrogenation of nitrobenzene over Pd catalysts (Figure 4a). Because MC functions as a hydrogen donor over EN selective catalysts, the activation of MC appears to determine the reaction rate in a manner similar to the previously discussed hydrogenation of nitrobenzene. In contrast, no apparent dependence was observed with AS-dominant Pd catalysts (Figure 6a, triangles) and Rh catalysts (Figure 6b).

Figure 7 shows the relationship between the formation rates of the products of (a) Pd and (b) Rh catalysts and the electronegativity of the second metal. A weak negative correlation was observed between the electronegativity of the second metal and the formation rate of EN (Figure 7a, circles), whereas that of AS increased as the electronegativity increased in both catalysts (Figures 7a and b, triangles). For Pd catalysts, the electronegativity of the second metal appears to play a significant role to determine the product distribution: a higher electronegativity makes the hydrogenation of the nitro group, which corresponds to the methanol-mediated CTH reaction,

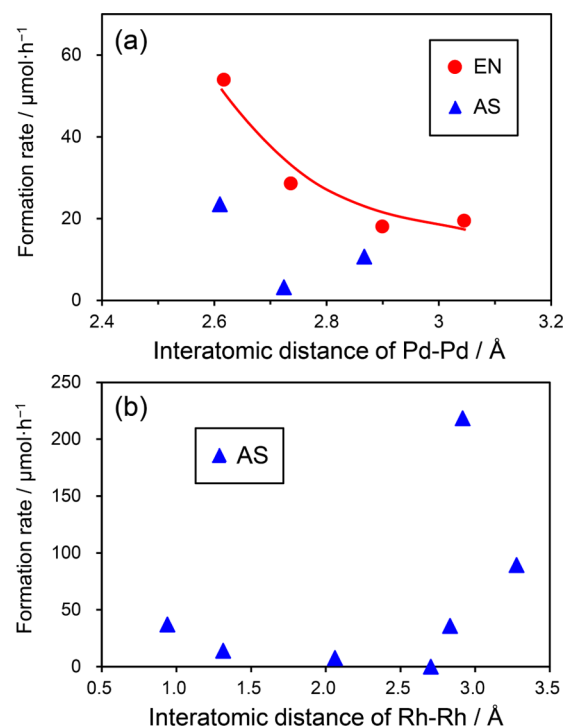


Figure 6. Dependences of the formation rate of the product on interatomic distance of (a) Pd–Pd of the Pd catalysts and (b) Rh–Rh of the Rh ones.

more favorable than that of the vinyl group. As discussed in section 3.2, the incorporation of the electronegative atoms suppresses C–H activation of MC but enhances O–H

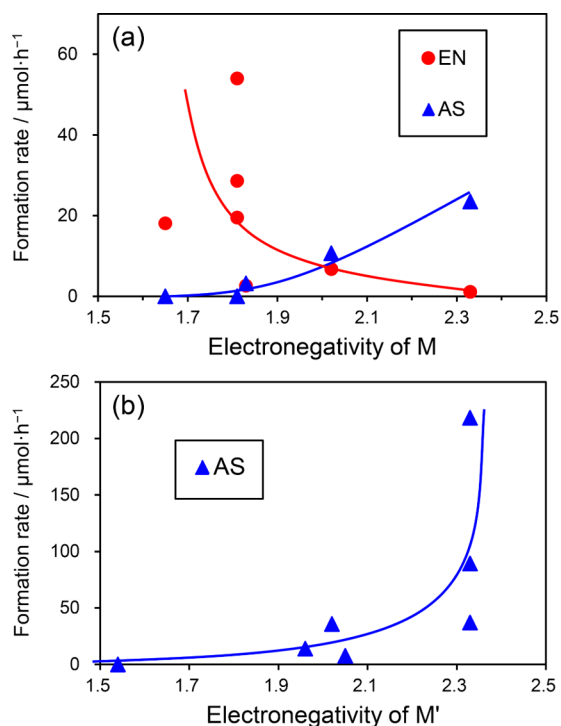


Figure 7. Relationship between the formation rate of the product and the electronegativity of the second metal elements of the (a) Pd and (b) Rh catalysts.

activation of methanol. Therefore, the results obtained using Pd catalysts (Figure 7a) are attributed to a change in the activation rate of each hydrogen donor. This concept can also be applied to the change in the catalytic activity of Rh catalysts. Notably, because the crystallite size of $\text{Pd}_{13}\text{Pb}_9$ is larger than that of other intermetallics, its true catalytic performance (specifically, the turnover frequency based on the number of exposed Pd atoms) appears to be much greater than those of other Pd catalysts. However, if so, the relationship between the catalytic activity and electronegativity is not changed because $\text{Pd}_{13}\text{Pb}_9$ is the most active investigated catalyst toward AS formation and is almost inactive toward EN formation.

Figure 8a describes the crystal structure of $\text{Pd}_{13}\text{Pb}_9$, where Pd and Pb atoms are arranged homogeneously and regularly. Typical facets of $\text{Pd}_{13}\text{Pb}_9$, (-223) and (623) , are also illustrated in Figure 8b; lattice diffractions of these facets were

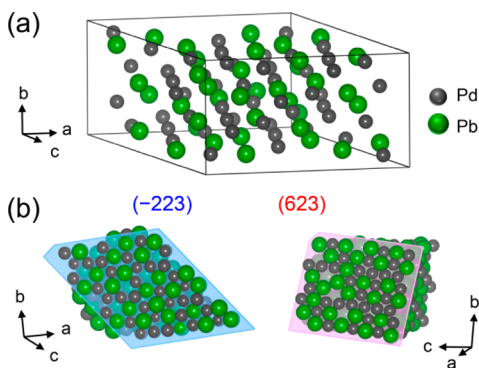


Figure 8. (a) Crystal structure of intermetallic $\text{Pd}_{13}\text{Pb}_9$ with the single unit cell in a monoclinic $C_{2/c}$ space group (PDF: #04-007-1453) and (b) its (-223) and (623) planes.

prominently observed at 38.8° and 39.9° in the XRD pattern of $\text{Pd}_{13}\text{Pb}_9$ (Figure 1a). Large Pd ensembles disappeared via the incorporation of Pb atoms, and these atoms are coadjacent at the atomic level. Thus, the intermetallic compound appears to provide the ideal platform for the chemoselective hydrogenation of NS.

To characterize the actual geometric and electronic states of the catalysts, we performed an FT-IR study of adsorbed CO molecules. Figure 9 shows the FT-IR spectra of CO adsorbed

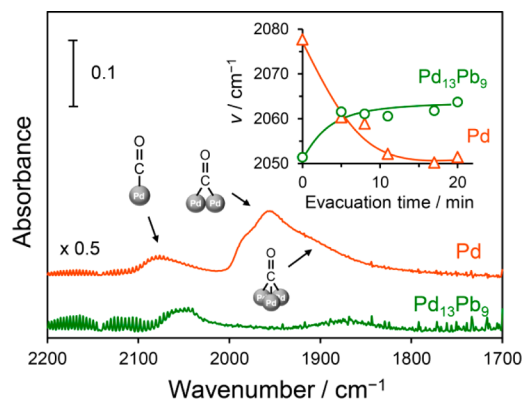


Figure 9. FT-IR spectra of CO adsorbed on Pd/SiO₂ and $\text{Pd}_{13}\text{Pb}_9/\text{SiO}_2$. Assignments of the peaks are illustrated: linear, bridged, and 3-fold coordination. Inset shows time course of the peak position assigned to the vibration of linear-type CO during evacuation at room temperature.

onto Pd and $\text{Pd}_{13}\text{Pb}_9$. The spectrum of monometallic Pd showed several peaks (at 2077, 1990–1930, and 1920–1870 cm^{-1}), which are assigned to C=O stretching vibrations of CO in linear, bridged, and 3-fold coordination modes, respectively.²⁸ A higher coordination number resulted in a lower wavenumber because of the enhancement of π back-donation to antibonding orbitals of C=O bond. A control experiment revealed that no peak was observed when CO was introduced onto Pb/SiO₂ (data not shown), thereby indicating that CO was not adsorbed onto Pb atoms. Bridged and 3-fold adsorptions were dominant on monometallic Pd, whereas linear adsorption was observed mainly on $\text{Pd}_{13}\text{Pb}_9$. The drastic decrease in the multicoordinated species can be interpreted to result from the disappearance of large Pd ensembles as a consequence of the formation of the intermetallic phase with Pb atoms.²⁹ Therefore, the obtained results are consistent with the intermetallic phase being exposed on the catalyst surface. The inset in Figure 9 shows the time course of the peak positions assigned to the linear-type CO during evacuation at room temperature. The peak positions changed and plateaued after 20 min of evacuation. This change is attributed to diminished dipole–dipole coupling between adsorbed CO molecules at high CO coverage.³⁰ Therefore, the final peak positions at sufficiently low CO coverage should reflect the true electronic states of Pd. The peak position of linearly adsorbed CO in the spectrum of $\text{Pd}_{13}\text{Pb}_9$ appeared at higher wavenumbers compared with that in the spectrum of Pd after saturation, indicating a lower electronic density of Pd atoms in $\text{Pd}_{13}\text{Pb}_9$ compared with those in monometallic Pd. This result is consistent with the results reported in the literature, in which an XPS analysis of the electronic state of Pd in Pd–Pb intermetallics supported on SiO₂ revealed that Pd became electron-deficient upon the formation of Pd–Pb intermetallic

phases.³¹ We also performed similar XPS measurements in the present study on monometallic Pd and Pd–Pb intermetallics. The peaks of Pd 3d_{5/2} and 3d_{3/2} emissions were shifted by 0.6 and 0.5 eV to higher binding energy, respectively, by the formation of Pd–Pb intermetallics (Supporting Information, Figure S2), which confirms that the formation of an intermetallic phase makes Pd electron-deficient. These results support the hypothesis that a charge transfer from Pd to Pb occurs via the formation of the intermetallics; hence, the polar sites are, indeed, constructed.

In this study, Pb-containing catalysts exhibited good catalytic performance. Pd–Pb catalysts that are so-called Lindlar catalysts are well-known to be effective for the semi-hydrogenation of alkynes to alkenes.³² The enhanced selectivity induced by Pb modification is considered to arise from the poisoning of the strong hydrogenation ability of Pd to be milder so that overhydrogenation is suppressed. In our case, in contrast, the role of Pb atoms is to provide new active Pd–Pb sites that are chemically different from the parent Pd. Pd–Pb catalysts are also used as effective catalysts in various aerobic oxidation systems. The direct oxidative esterification of methacrolein to methyl methacrylate (MMA) using Pd₃Pb has been commercialized as an industrial process.³³ In this system, Pb inhibits undesired side reactions, such as the decarbonylation of methacrolein to enhance the product selectivity. We recently discovered that Pd₃Pb exhibits much higher catalytic activity than monometallic Pd in the oxidative dehydrogenation of an amine to an imine.³⁴ A kinetic study revealed that Pd₃Pb phase accelerated the desorption of imine, which was the late-determining step. Thus, although Pd–Pb catalysts exhibit unique catalytic properties in various catalytic systems, the roles of Pb in the reported Pd–Pb systems differ among the systems and from that in the present study.

CONCLUSION

In this study, a series of Pd- and Rh-based intermetallic compounds supported on silica were prepared, and their catalytic properties in the CTH reactions of nitrobenzene and NS were investigated. The formation of the intermetallic compounds makes an ideal platform for the chemoselective hydrogenation of NS: two metal elements are coadjacent at the atomic level on the surface of the nanoparticles. An increase in the electronegativity of the second metal element provides polar sites and enhances the activation of methanol as a hydrogen donor, which accelerates the hydrogenation of the nitro group of NS and hence improves the yield of AS. Over Rh catalysts, AS is selectively formed as a result of the absence of MC activation ability. Pd₁₃Pb₉ exhibits the highest chemoselectivity in the conversion of NS to AS (92%) among Pd catalysts. In addition to NS, various nitroaromatic compounds having olefinic bonds were selectively converted into the corresponding amino derivatives within 1 or 1.5 h using PdRh₂. Moreover, RhPb₂ not only exhibits high selectivity toward AS (93%) but also exhibits the highest NS conversion (94%). This catalyst also gives high selectivity toward AS (91%), even when H₂ is used as a hydrogen source. Thus, the present study demonstrates the excellence of these catalysts in chemoselective hydrogenation and the validity of the strategy of employing these intermetallic compounds. The obtained insights open the opportunity to develop more efficient and well-structured catalytic systems for selective conversion reactions.

ASSOCIATED CONTENT

Supporting Information

Results of the self-CTH reaction of MC, time course of conversion and selectivity in CTH reaction of NS, XPS. This material is available free of charge via the Internet at <http://pubs.acs.org>.

AUTHOR INFORMATION

Corresponding Authors

*Phone: +81-3-5734-2602. Fax: +81-3-5734-2758. E-mail: furukawa.s.af@m.titech.ac.jp.

*Phone: +81-3-5734-3532. Fax: +81-3-5734-2758. E-mail: komatsu.t.ad@m.titech.ac.jp.

Notes

Notes. The authors declare no competing financial interest. The authors declare no competing financial interest.

ACKNOWLEDGMENTS

This work was supported by JSPS KAKENHI Grant No. 23360353. We thank the Center for Advanced Materials Analysis Tokyo Institute of Technology for their assistance in TEM analysis.

REFERENCES

- (1) Downing, R. S.; Kunkeler, P. J.; vanBekum, H. *Catal. Today* **1997**, *37*, 121–136.
- (2) Suchy, M.; Winternitz, P.; Zeller, M. World Patent 91/00278, 1991.
- (3) Burawoy, A.; Critchley, J. P. *Tetrahedron* **1959**, *5*, 340–351.
- (4) Kovar, F.; Armond, F. E. U.S. Patent 3,975,444, 1976.
- (5) Butera, J.; Bagli, J. World Patent 91/09023, 1991.
- (6) Rylander, P. N. *Catalytic Hydrogenation in Organic Synthesis*; Academic Press: New York, 1979.
- (7) Corma, A.; Serna, P. *Science* **2006**, *313*, 332–334.
- (8) Shimizu, K.; Miyamoto, Y.; Kawasaki, T.; Tanji, T.; Tai, Y. *J. Phys. Chem. C* **2009**, *113*, 17803–17810.
- (9) Mitsudome, T.; Mikami, Y.; Matoba, M.; Mizugaki, T.; Jitsukawa, K.; Kaneda, K. *Angew. Chem., Int. Ed.* **2012**, *51*, 136–139.
- (10) Shimizu, K.; Miyamoto, Y.; Satsuma, A. *J. Catal.* **2010**, *270*, 86–94.
- (11) Bullock, R. M. *Chem.–Eur. J.* **2004**, *10*, 2366–2374.
- (12) Westbrook, J. H.; Fleischer, R. L. *Magnetic, Electrical and Optical Properties and Applications of Intermetallic Compounds*; Wiley: New York, 2000.
- (13) Galloway, E.; Armbruster, M.; Kovnir, K.; Tikhov, M. S.; Lambert, R. M. *J. Catal.* **2009**, *261*, 60–65.
- (14) Johnstone, R. A. W.; Wilby, A. H. *Tetrahedron* **1981**, *37*, 3667–3670.
- (15) Sala, R.; Doria, G.; Passarotti, C. *Tetrahedron Lett.* **1984**, *25*, 4565–4568.
- (16) Tike, M. A.; Mahajani, V. V. *Chem. Eng. J.* **2006**, *123*, 31–41.
- (17) Cristina, M.; Oliveira, F. *Appl. Catal., A* **2007**, *329*, 7–15.
- (18) Johnstone, R. A. W.; Wilby, A. H.; Entwistle, I. D. *Chem. Rev.* **1985**, *85*, 129–170.
- (19) Allred, A. L. *J. Inorg. Nuclear Chem.* **1961**, *17*, 215–221.
- (20) Allred, A. L.; Rochow, E. G. *J. Inorg. Nuclear Chem.* **1958**, *5*, 264–268.
- (21) Shriver, D. F.; Atkins, P. W. *Inorganic Chemistry*; 3rd ed.; Oxford University Press: Oxford, 1999.
- (22) Greeley, J.; Mavrikakis, M. *J. Am. Chem. Soc.* **2002**, *124*, 7193–7201.
- (23) Desai, S. K.; Neurock, M.; Kourtakis, K. *J. Phys. Chem. B* **2002**, *106*, 2559–2568.
- (24) Beste, A.; Mullins, D. R.; Overbury, S. H.; Harrison, R. J. *Surf. Sci.* **2008**, *602*, 162–175.

- (25) Feng, G.; Huo, C. F.; Deng, C. M.; Huang, L.; Li, Y. W.; Wang, J. G.; Jiao, H. J. *J. Mol. Catal. A: Chem.* **2009**, *304*, 58–64.
- (26) Branda, M. M.; Collins, S. E.; Castellani, N. J.; Baltanas, M. A.; Bonivardi, A. L. *J. Phys. Chem. B* **2006**, *110*, 11847–11853.
- (27) Huang, L.; Zhu, Y. L.; Huo, C. F.; Zheng, H. Y.; Feng, G.; Zhang, C. H.; Li, Y. W. *J. Mol. Catal. A: Chem.* **2008**, *288*, 109–115.
- (28) Kim, W. J.; Shin, E. W.; Kang, J. H.; Moon, S. H. *Appl. Catal., A* **2003**, *251*, 305–313.
- (29) Wei, T.; Wang, J.; Goodman, D. W. *J. Phys. Chem. C* **2007**, *111*, 8781–8788.
- (30) Primet, M.; Demenorval, L. C.; Fraissard, J.; Ito, T. J. *Chem. Soc. Faraday Trans. 1* **1985**, *81*, 2867–2874.
- (31) Hirano, T.; Kazahaya, Y.; Nakamura, A.; Miyao, T.; Naito, S. *Catal. Lett.* **2007**, *117*, 73–78.
- (32) Lindlar, H. *Helv. Chim. Acta* **1952**, *35*, 446–456.
- (33) Yamamatsu, S.; Yamaguchi, T.; Yokota, K.; Nagano, O.; Chono, M.; Aoshima, A. *Catal. Surv. Asia* **2010**, *14*, 124–131.
- (34) Furukawa, S.; Suga, A.; Komatsu, T. *Chem. Commun.* **2014**, *50*, 3277–3280.